ACS OMEGA

http://pubs.acs.org/journal/acsodf

Article

Study of the Variation of the Electronic Distribution and Motional Dynamics of Two Independent Molecules of an Asymmetric Unit of Atorvastatin Calcium by Solid-State NMR Measurements

Krishna Kishor Dey, Lekhan Lodhi, and Manasi Ghosh*

Cite This: *ACS Omega* 2021, 6, 22752–22764

Read Online

ACCESS | Metrics & More | Article Recommendations | Supporting Information

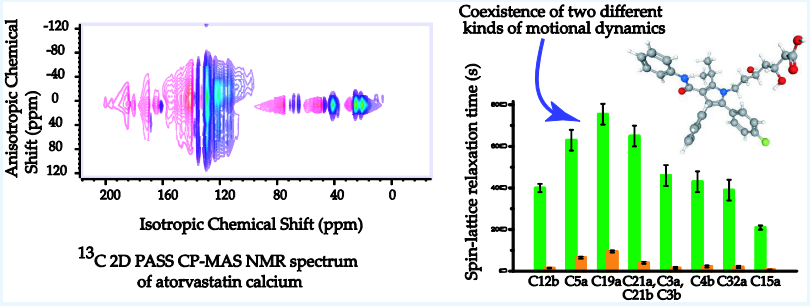

ABSTRACT: Significant changes in the spin-lattice time and chemical shift anisotropy (CSA) parameters are observed in two independent molecules of an asymmetric unit of atorvastatin calcium (ATC-I) (which is referred to as "a"- and "b"-type molecules by following Wang et al.). The longitudinal magnetization decay curve is fitted by two exponentials—one with longer relaxation time and another with shorter relaxation time for most of the carbon nuclei sites. The local correlation time also varies significantly. This is the experimental evidence of the coexistence of two different kinds of motional degrees of freedom within ATC-I molecule. The solubility and bioavailability of the drug molecule are enhanced due to the existence of two different kinds of dynamics. Hence, the macroscopic properties like solubility and bioavailability of a drug molecule are highly correlated with its microscopic properties. The motional degrees of freedom of "a"- and "b"-type molecules are also varied remarkably at certain carbon nuclei sites. This is the first time the change in the molecular dynamics of two independent molecules of an asymmetric unit of atorvastatin calcium is quantified using solid-state NMR methodology. These types of studies, in which the chemical shift anisotropy (CSA) parameters and spin-lattice relaxation time provide information about the change in electronic distribution and the spin dynamics at the various crystallographic location of the drug molecule, will enrich the field "NMR crystallography". It will also help us to understand the electronic distribution around a nucleus and the nuclear spin dynamics at various parts of the molecule, which is essential to develop the strategies for the administration of the drug.

1. INTRODUCTION

Atorvastatin is an inhibitor of the 3-hydroxy methylglutaryl coenzyme A (HMG-CoA) reductase enzyme, which participates in the conversion of HMG-CoA to mevalonate. It is used to reduce the elevated total cholesterol, low-density lipoprotein cholesterol (LDL-C), apolipoprotein B (apo B), and triglyceride (TG) levels, as well as to increase the high-density lipoprotein cholesterol (HDL-C) level. Atorvastatin calcium exists in several polymorphic forms due to the variation of density of packing and hydrogen-bond network.[1] Among them, Form I of ATC (ATC-I) has the most stable crystalline form.[1] The therapeutic efficacy of a drug, especially the rate of absorption in the digestive tract, depends on the polymorphic state. The solubility, melting point, density, hardness, crystal shape, vapor pressure, and optical and electrical properties are also altered with the polymorphic states of a compound.[1] The bioavailability of the drug depends on the solubility, dissolution, density, flow properties, and shape of crystals. Hence, it is necessary to have a detailed picture of the drug molecule for the accountability of its efficacy, stability, and bioavailability. High-resolution solid-state nuclear magnetic resonance (NMR) spectroscopy is an indispensable technique to analyze biomolecules. The target of this work is to study the change in the structure and dynamics of two independent molecules of an asymmetric unit of the atorvastatin calcium (ATC-I) by applying solid-state NMR methodology.

Wang et al.[1] determined the chemical shift tensors of ATC-I at crystallographically different carbon sites and fluorine sites by

Received: June 12, 2021
Accepted: August 16, 2021
Published: August 26, 2021

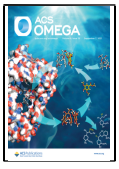

density functional theory (DFT). Holmes et al.[2] determined the structure of the local calcium-ligand coordination environment of atorvastatin calcium by experiment and computation. They extracted the chemical shift tensor, quadrupolar coupling tensor, and the Euler angles by ^{43}Ca solid-state NMR. The polymorphic form of atorvastatin calcium (ATC) can be distinguished by the line shape of the ^{43}Ca solid-state nuclear magnetic resonance (SSNMR) spectrum.[3] Although the values of chemical shift anisotropy (CSA) parameters of ATC-EG and ATC-I were comparable, but it was indicated by the quadrupolar parameters that the local point symmetries near the calcium sites of ATC-I and ATC-EG are different. The goal of the present work is to determine the principal components of the CSA tensor of two independent molecules of ATC-I (referred to as "a"- and "b"-type molecule) by two-dimensional phase-adjusted spinning sideband (2DPASS) cross-polarization magic angle spinning (CP-MAS) solid-state nuclear magnetic resonance (SSNMR) experiments.[4,5] ^{13}C 2DPASS CP-MAS SSNMR spectroscopy was used to find the principal components of CSA parameters of charge-transfer co-crystal, biopolymers, and drug molecules.[6−16] The molecular dynamics of "a" and "b" types of molecules (the types "a" and "b" nomenclature is according to Wang et al.[1]) is determined by measuring ^{13}C spin-lattice relaxation time by the Torchia CP method and by calculating the molecular correlation time at crystallographically different locations of carbon nuclei.

2. RESULT AND DISCUSSION

2.1. Determination of Chemical Shift Anisotropy (CSA) Tensor of Two Independent Molecules of an Asymmetric Unit of Atorvastatin Calcium. ATC-I is the most stable crystalline form among various polymorphic states of atorvastatin calcium.[29−32] Wang et al.[1] evaluated the CSA tensor by DFT calculations. We have measured principal components of the CSA tensor of 33 crystallographically different carbon nuclei of "a"- and "b"-type molecules by ^{13}C 2DPASS CP-MAS SSNMR experiments. We have also observed two well-resolved resonance lines for certain carbon nuclei sites corresponding to two different molecules of the asymmetric unit as previously reported by Wang et al.[1] Figure 1a,b shows the structure and ^{13}C CP-MAS SSNMR spectrum of ATC-I at a MAS frequency of 10 kHz, respectively. The assignment of various carbon nuclei positions for "a"- and "b"-type molecules is done by following Wang et al.[1] Figure 2 shows the ^{13}C 2DPASS CP-MAS SSNMR spectrum at a MAS frequency of 2 kHz. The double-resonance lines signify the coexistence of the two molecules ("a"- and "b"-type molecules) within the asymmetric unit of ATC-I. The difference in isotropic chemical shift between various carbon nuclei of "a"- and "b"-type molecules arises due to the asymmetric crystal packing, the presence of the strong intermolecular and intramolecular hydrogen bonding, and the electrostatic interactions between the calcium ion and the carboxyl groups.[1]

From Table 1, it is clear that the spinning CSA sideband patterns of C16a, C16b, C12a, C20a, C20b, C24a, and C24b are nearly axially symmetric because the value of the asymmetry parameter $\left(\eta = \frac{\delta_{22} - \delta_{11}}{\delta_{33} - \delta_{iso}}\right)$ for those carbon nuclei sites are $\eta \leq 0.3$. The asymmetry (η) parameter measures the deviation of the spinning CSA sideband pattern from its axially symmetric shape.[35] The orientation of the asymmetric pattern is monitored by "skew" $\left(k = \frac{3(\delta_{22} - \delta_{iso})}{\Omega}\right)$. For most of the carbon nuclei like C35b, C33a, C9a, C9b, C7a, C7b, C6a, C6b, C11a, C11b, C8a,

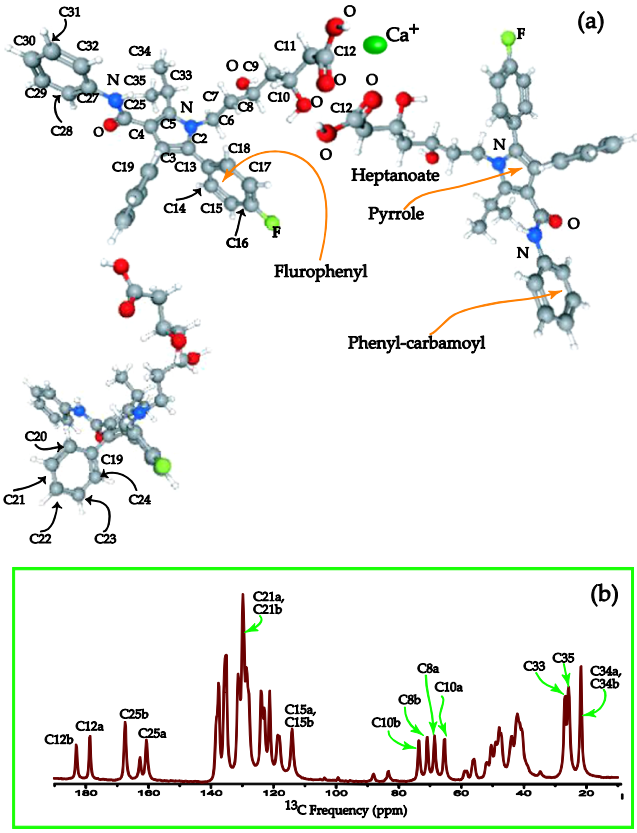

Figure 1. (a) Atorvastatin calcium molecule and (b) ^{13}C CP-MAS SSNMR spectrum of atorvastatin calcium.

C8b, C10a, C10b, C31a, C31b, C29a, C29b, C2a, C2b, C13a, C13b, C21a, C21b, C23a, C23b, C18a, C18b, C27b, C5a, and C25b, the spinning CSA sideband pattern is highly asymmetric. The anisotropy parameter $\Delta\delta = \delta_{33} - \frac{(\delta_{11} + \delta_{22})}{2}$ defines the largest separation of the spinning CSA sideband pattern from the center of gravity ($\delta_{iso} = (\delta_{11} + \delta_{22} + \delta_{33})/3$). The span ($\Omega = \delta_{11} - \delta_{33}$) represents the width of the spinning CSA sideband pattern. Remarkable variations of the width of the spinning CSA sideband pattern and the asymmetry parameter between "a"- and "b"-type molecules are observed for C2, C5, C9, C11, and C18 carbon nuclei (Table 1). The difference in CSA parameters signifies the variation of the electron charge distribution in two independent molecules of the asymmetric unit of ATC-I.

Table 1 shows that the isotropic chemical shift, as well as the anisotropic chemical shift, is highest for the heptanoate carbonyl carbon (C12) and the amide carbonyl carbon (C25) due to the magnetic anisotropy. In the principal axes system (PAS), there are three different magnetic susceptibilities (X_x, X_y, X_z) along three mutually perpendicular directions of the nonsymmetric carbonyl group carbons C12 and C25. According to the McConnell equation,[52] the magnetic anisotropy appears due to two anisotropic susceptibilities—one parallel to the magnetic field ($\Delta X_{\parallel} = X_z - X_x$) and another perpendicular to the magnetic field ($\Delta X_{\perp} = X_y - X_x$); $\delta_{anis} = \{\Delta X_{\parallel}(3\cos^2\theta_1 - 1) + \Delta X_{\perp}(3\cos^2\theta_2 - 1)\}/3R^3$, where θ_1 and θ_2 are the angles subtended by the radius vector with the x-axis and z-axis, respectively.[52] The polar bond of the carbonyl group is another source of the large values of CSA parameters.[52,53] The experimental value of δ_{22} associated with the carbonyl group carbon is the most sensitive to a change in the hydrogen bonding associated with the group. The

https://doi.org/10.1021/acsomega.1c03095
ACS Omega 2021, 6, 22752−22764

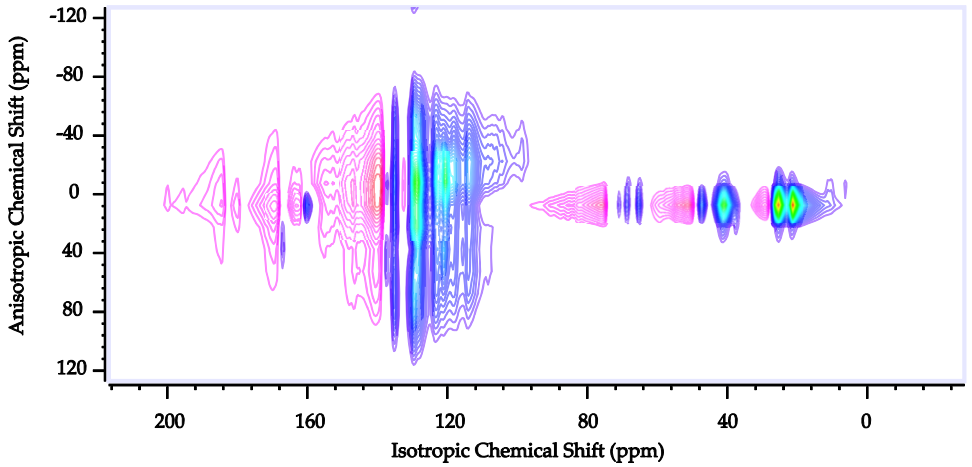

Figure 2. ^{13}C 2DPASS CP-MAS SSNMR spectrum of atorvastatin calcium.

principal component of the CSA tensor δ_{22} shifted linearly toward the higher-frequency side with the decrease of hydrogen bonding.[49,54] The values of δ_{22} are 193.8 and 180.6 ppm, respectively, of C25 amide carbonyl group carbon for "a"- and "b"-type molecules of atorvastatin calcium, indicating that the intramolecular hydrogen bonding (N−H·····O) associated with "a"-type molecule is decreased compared to the "b"-type molecule. Hence, measurement of the principal components of the CSA parameters also provides the signature of the change in the hydrogen bonding in two independent molecules of an asymmetric unit of atorvastatin calcium.

Atorvastatin calcium molecule consists of phenyl ring, phenyl carbamoyl, fluorophenyl, pyrarole, and heptanoate. The aromatic heterocycle pyrroles are considered fundamental for the design of new anti-inflammatory, anti-nociceptive, anti-microbial, analgesic, antitumor, antiepileptic, antiviral, anti-hypertension, and antidiabetic agents. The spinning CSA sideband patterns at various carbon nuclei sites of the phenyl ring, phenyl carbamoyl, fluorophenyl, pyrrole, and heptanoate are shown in Figures 3−7, respectively. Remarkable variations of "span" and "anisotropy" parameters are observed for "a"- and "b"-type molecules at C9 and C11 carbon nuclei sites (reside on heptanoate). The values of span are 43.6 and 82.2 ppm for C9b and C9a, respectively. The anisotropy parameter is −32.7 ppm for C9b and 65.7 ppm for C9a. The "span" is 46.6 ppm for C11b and 82.2 ppm for C11a. The anisotropy parameter is 36.5 and 65.2 ppm for C11b and C11a, respectively.

The span and anisotropy parameters of C2, C4, C5 carbon nuclei residing on the pyrrole ring vary widely for "a"- and "b"-type molecules. It is not possible to measure the difference of CSA parameters of "a"- and "b"-type molecules of C3 nuclei (reside on pyrrole ring) because the isotropic chemical shift of two molecules overlapped with each other at 123.6 ppm. A significant variation of the spin-lattice relaxation time is observed for two molecules at C2 and C5 carbon nuclei sites.

Figure 5 shows the spinning CSA sideband patterns of the carbon nuclei residing on the fluorophenyl ring. Remarkable variation of the spinning CSA sideband patterns is observed at C14, C18 nuclei sites of "a"- and "b"-type molecules. The isotropic chemical shifts of C14, C18 nuclei are overlapped with each other; hence, it is only possible to find the average values of CSA parameters for C14a, C18a, and C14b, C18b nuclei. The values of span are 139.7 and 201 ppm, respectively, for C14b, C18b, and C14a, C18a. The anisotropy parameters are 112.7 and 160.4 ppm for C14b, C18b, and C14a, C18a, respectively. Generally, the values of CSA parameters are large for the carbon nuclei residing on the aromatic ring due to magnetic shielding and deshielding effect. A magnetic field is induced along the direction of the external magnetic field when π electrons revolve in the clockwise direction. As a result, the effective magnetic field experienced by the nucleus is increased; this phenomenon is known as the deshielding effect. On the contrary, a magnetic field is induced along the opposite direction of the external magnetic field when π electrons revolve in the counterclockwise direction. As a consequence, the effective magnetic field experienced by the nucleus is decreased; this phenomenon is known as the shielding effect. Hence, the chemical shift is high for carbon nuclei surrounded by nonbonded π electrons. But the values of "asymmetry" and span are substantially lower for C16 nucleus (bonded with fluorine atom) residing on the fluorophenyl ring compared to other nuclei. The transfer of electron density from the carbon−hydrogen or carbon−carbon(C−H or C−C) σ-orbital to adjacent carbon−fluorine (C−F) antibonding σ^* orbital is known as hyperconjugation. As fluorine is more electronegative than carbon and hydrogen, the carbon−hydrogen or carbon−carbon σ-orbital acts as an electron donor and carbon−fluorine σ^* orbital acts as an electron acceptor.[55−59] As a result, an electron density is built up around the C16 carbon nucleus and the shielding effect is increased. Hence, the electron delocalization associated with hyperconjugation is the reason for the lower values of CSA parameters for C16 carbon nuclei. This effect is known as the Gauche effect.[56]

2.2. Theory to Explain Experimental Findings. In the presence of an external magnetic field, the electrons revolving around a nucleus produce a secondary magnetic field, which has the potential to change the Larmor precession frequency of the nucleus. This interaction of the secondary magnetic field with the nucleus is known as the shielding interaction. The change in the resonance frequency caused by this interaction is referred to as the chemical shift. The chemical shift frequency can be expressed as $\omega(\theta,\Phi) = -\omega_0 (\delta_{11} \sin^2\theta \cos^2\Phi + \delta_{22} \sin^2\theta \sin^2\Phi + \delta_{33} \cos^2\theta)$, where θ and Φ are the polar and azimuthal angles with respect to the direction of the applied magnetic field ($\mathbf{B_0}$) in the principal axis system (PAS), respectively. All values of θ and Φ are possible in a powder sample. Each different molecular orientation implies a different orientation of PAS with respect to the external magnetic field as the PAS is fixed in the molecule. A

https://doi.org/10.1021/acsomega.1c03095
ACS Omega 2021, 6, 22752−22764

Table 1. Chemical Shift Anisotropy Parameters of Atorvastatin Calcium at Crystallographically Different Carbon Nuclei Sites Measured by the 2DPASS CP-MAS SSNMR Experiment

CSA parameters of atorvastatin calcium								
carbon from different chemical environment	δ_{11} (ppm)	δ_{22} (ppm)	δ_{33} (ppm)	δ_{iso} (ppm)	anisotropy (ppm) $\Delta\delta = \delta_{33} - \frac{(\delta_{11} + \delta_{22})}{2}$	asymmetry $\eta = \frac{\delta_{22} - \delta_{11}}{\delta_{33} - \delta_{iso}}$	skew $k = \frac{3(\delta_{22} - \delta_{iso})}{\Omega}$	span (ppm) $\Omega = \delta_{11} - \delta_{33}$
C12b	260.8 ± 1.1	162.1 ± 0.7	126.9 ± 0.9	182.74	116.3 ± 1.7	0.4	−0.5	133.9 ± 0.9
C12a	249.9 ± 1.2	153.7 ± 0.7	131.7 ± 0.9	178.46	107.1 ± 1.7	0.3	−0.6	118.1 ± 1.0
C25b	241 ± 1.1	180.6 ± 0.7	81.4 ± 0.8	167.49	−129.4 ± 1.2	0.7	0.2	159.5 ± 0.9
C25a	232.7 ± 1.1	193.8 ± 0.7	74.7 ± 0.6	167.07	−138.5 ± 2.1	0.4	0.5	157.9 ± 0.6
C16b	175.7 ± 0.9	169.1 ± 0.6	135.3 ± 0.7	160.04	−37.1 ± 1.1	0.2	0.7	40.4 ± 0.8
C16a	175.7 ± 0.7	169.2 ± 0.5	135.6 ± 0.6	160.19	−36.8 ± 0.9	0.2	0.7	40.1 ± 0.6
C5b	224 ± 2.6	117.8 ± 1.7	71.6 ± 2	137.82	129.2 ± 3.9	0.5	0.4	152.3 ± 2.1
C5a	247.2 ± 2.1	118.5 ± 1.4	45.8 ± 1.5	137.19	165 ± 3.1	0.7	−0.3	201.4 ± 1.4
C19b, C27a	250.5 ± 1.4	109.9 ± 0.9	45.3 ± 1.0	135.23	172.9 ± 2.1	0.5	−0.4	205.2 ± 1.0
C19a	249.8 ± 2.4	109.8 ± 1.6	47.1 ± 1.8	135.58	171.3 ± 3.6	0.5	−0.4	202.6 ± 0.6
C27b	247.1 ± 1.8	118.3 ± 1.2	38.9 ± 1.4	134.79	168.4 ± 2.8	0.7	−0.2	208.1 ± 1.2
C20a, C20b, C24a, C24b	243.8 ± 2	190.4 ± 6.7	40.9 ± 7.3	131.09	−258 ± 4.5	0.3	−0.2	202.9 ± 1.2
C18b, C14b	205.9 ± 3.4	120.1 ± 2.2	66.2 ± 2.6	130.74	112.7 ± 5.1	0.7	−0.2	139.7 ± 3
C18a, C14a	237.4 ± 4	117.7 ± 2.7	36.4 ± 3.0	130.5	160.4 ± 6	0.7	−0.2	201 ± 2.5
C21a, C21b, C23a, C23b	243.1 ± 1.7	113.6 ± 1.1	31.7 ± 1.2	129.47	170.5 ± 2.5	0.7	−0.2	211.4 ± 1.1
C13a	243.3 ± 1.7	113.8 ± 1.1	31.9 ± 1.2	129.69	170.5 ± 2.5	0.7	−0.2	211.4 ± 1.1
C13b	237.1 ± 2.3	116.6 ± 1.5	33.6 ± 1.7	129.1	161.9 ± 3.4	0.7	−0.2	203.4 ± 1.5
C2b	233.9 ± 3.2	116.5 ± 2.2	34.1 ± 2.4	128.17	158.7 ± 4.8	0.8	−0.2	199.9 ± 2.1
C2a	206.4 ± 2.8	123.5 ± 1.8	55.6 ± 2.2	128.51	116.9 ± 4.2	0.8	−0.1	150.8 ± 2.3
C31a, C31b, C29a, C29b	235.7 ± 2.8	115.5 ± 1.9	31.5 ± 2.1	127.56	162.2 ± 4.3	0.8	−0.2	204.2 ± 1.8
C3a, C3b, C22a, C22b	222.4 ± 3.2	104.2 ± 2.1	44.3 ± 2.4	123.63	148.1 ± 4.9	0.6	−0.3	178.1 ± 2.3
C30a, C30b	216.8 ± 3	103.7 ± 2	49 ± 2.2	123.22	140.5 ± 4.5	0.6	−0.3	167.8 ± 2.2
C4b	198.6 ± 1.2	103.2 ± 0.7	60.9 ± 0.9	120.92	116.5 ± 1.8	0.5	−0.4	137.7 ± 1
C4a	210.3 ± 2.5	102.4 ± 1.6	55 ± 1.9	122.57	131.6 ± 3.8	0.5	−0.4	155.3 ± 2
C32b, C28b	218.9 ± 2.4	93.4 ± 1.6	40.9 ± 1.8	117.76	151.7 ± 3.6	0.5	−0.4	178.0 ± 1.7
C32a, C28a	218.4 ± 2.4	94.5 ± 1.6	41.9 ± 1.8	118.28	150.2 ± 3.6	0.5	−0.4	175.0 ± 1.2
C15b, C17b	216.5 ± 2.1	88.0 ± 1.4	36.6 ± 1.6	113.68	154.2 ± 3.2	0.5	−0.4	179.9 ± 1.5
C15a, C17a	217.0 ± 2.5	91.4 ± 1.7	33.3 ± 1.9	113.90	154.7 ± 3.8	0.5	−0.4	183.7 ± 1.8
C10b	101 ± 0.6	69.7 ± 0.4	48.6 ± 0.5	73.11	41.9 ± 0.9	0.7	−0.2	52.5 ± 0.5
C10a	93.2 ± 0.7	62.1 ± 0.5	39.4 ± 0.5	64.9	42.5 ± 1.1	0.8	−0.1	53.8 ± 0.5
C8b	100.6 ± 1.3	67.9 ± 0.8	42.8 ± 0.9	70.45	45.3 ± 1.9	0.8	−0.1	57.8 ± 0.8
C8a	100.6 ± 0.8	62.8 ± 0.6	40.8 ± 0.6	68.12	48.8 ± 1.3	0.7	−0.3	59.8 ± 0.3
C11b	72.9 ± 1.0	46.5 ± 0.6	26.4 ± 0.7	48.6	36.5 ± 1.5	0.8	−0.1	46.6 ± 0.6
C11a	90.9 ± 2.7	42.6 ± 1.9	8.7 ± 2	47.41	65.2 ± 4.1	0.8	−0.2	82.2 ± 1.2
C6b	59.4 ± 0.6	41.5 ± 0.2	21.1 ± 0.5	40.68	−29.3 ± 0.4	0.9	0.06	38.2 ± 0.4
C6a	64.5 ± 0.4	45.3 ± 0.3	20 ± 0.2	43.3	−34.8 ± 0.2	0.8	0.1	44.4 ± 0.5
C7b	61.9 ± 0.6	42.5 ± 0.4	21.4 ± 0.4	41.97	−30.8 ± 0.7	0.9	0.04	40.5 ± 0.5
C7a	58.7 ± 0.4	40.5 ± 0.2	20.8 ± 0.3	40.02	−28.8 ± 0.5	0.9	0.04	37.9 ± 0.4
C9b	63.5 ± 0.4	41.7 ± 0.3	19.9 ± 0.2	41.53	−32.7 ± 0.2	1	0	43.6 ± 0.5
C9a	90.5 ± 0.4	41.3 ± 0.3	8.4 ± 0.2	46.73	65.7 ± 0.2	0.7	−0.2	82.2 ± 0.4
C33b	36.1 ± 0.5	29.7 ± 0.2	13.3 ± 0.3	26.41	−19.6 ± 0.1	0.5	0.4	22.8 ± 0.2
C33a	40.1 ± 0.4	26.6 ± 0.3	12 ± 0.2	26.25	−21.3 ± 0.1	0.9	0.4	28.0 ± 0.2
C35b	46.8 ± 0.5	22.1 ± 0.2	6.8 ± 0.3	25.26	32.4 ± 0.1	0.7	−0.2	40.0 ± 0.2
C35a	47.4 ± 0.4	20.8 ± 0.3	6.7 ± 0.2	24.97	33.7 ± 0.1	0.6	−0.3	40.7 ± 0.2
C34b	36.9 ± 0.3	19.4 ± 0.2	7.5 ± 0.2	21.27	23.5 ± 0.4	0.7	−0.2	29.4 ± 0.3
C34a	47.4 ± 0.4	20.8 ± 0.3	6.7 ± 0.2	21.23	23.8 ± 0.4	0.7	−0.2	29.8 ± 0.3

different chemical shift is associated with each orientation of the molecule. Therefore, the spectrum (as shown in Figure 3a) takes the shape of a powder pattern with lines from the different molecular orientations. The intensity at a particular frequency is proportional to the number of molecular orientations with a particular chemical shift. The shape of the powder pattern depends on the symmetry of the CSA tensor, i.e., on the symmetry surrounding the nucleus. The CSA tensor can be represented by an ellipsoid (as shown in Figure 4a) fixed within the molecule and centered on the nucleus. The principal axes of the ellipsoid coincide with the principal axis system (PAS) of the CSA tensor, and the length of each principal axis of the ellipsoid is proportional to the principal value of the CSA tensor. The nuclear frequency resonates at the lowest value of the magnetic field when the narrowest part of the ellipsoid is along the direction of the applied magnetic field, i.e., when the nuclear shielding effect is lowest. On the other hand, the nuclear frequency resonates at the highest value of the magnetic field when the widest part of the ellipsoid is along the direction of the applied magnetic field, i.e., when the nuclear shielding effect is

https://doi.org/10.1021/acsomega.1c03095
ACS Omega 2021, 6, 22752−22764

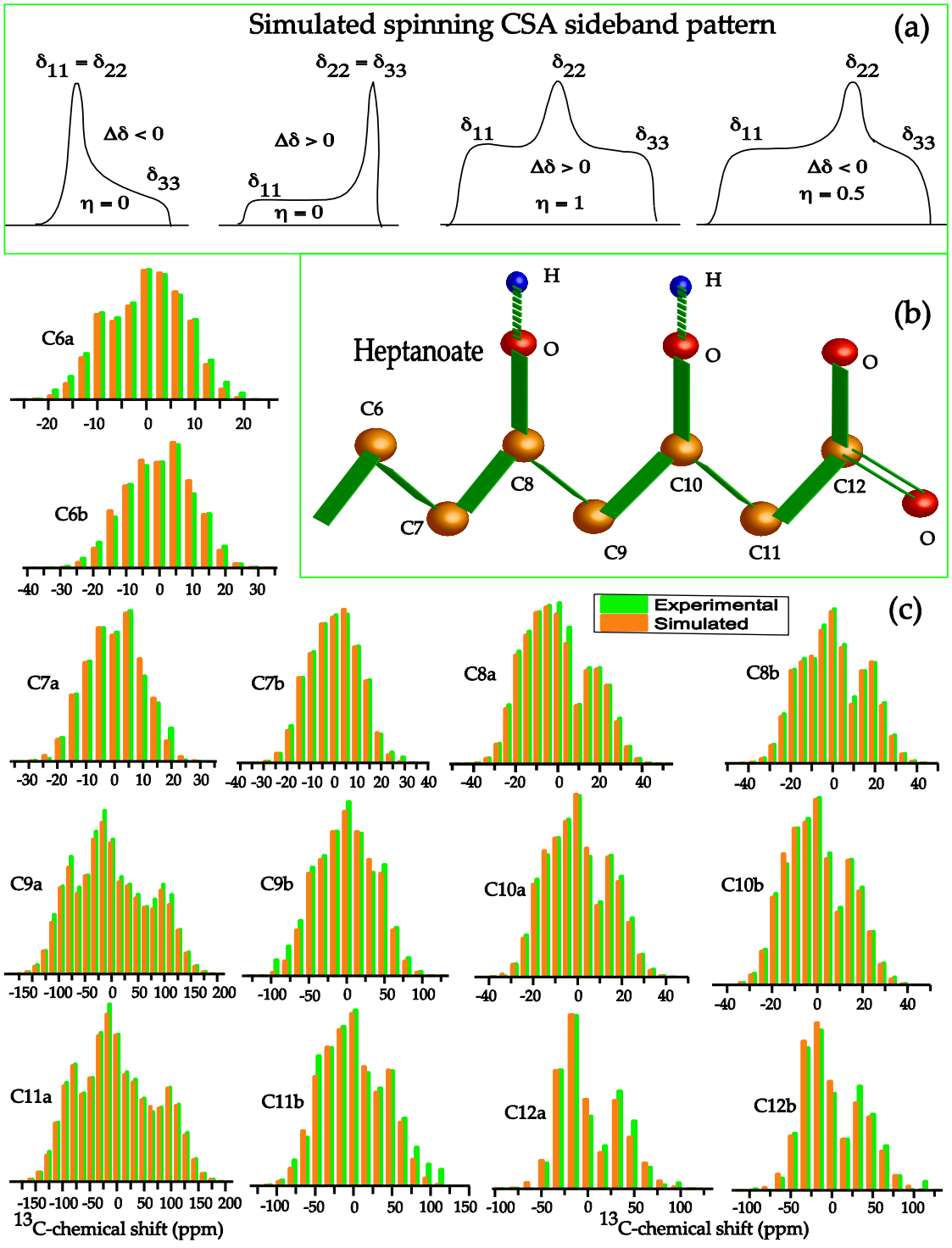

Figure 3. (a) Simulated spinning CSA sideband pattern. (b) Chemical structure of heptanoate. (c) Spinning CSA sideband patterns of C6, C7, C8, C9, C10, C11, and C12 nuclei.

highest.[33−51] The direction of the ellipsoid is changed with the orientation of the molecule. The principal components of the CSA tensor can provide information about the symmetry of the electron distribution surrounding the nucleus. If the nucleus is at an axially symmetric site, then the value of the asymmetry parameter $\eta = \frac{\delta_{22} - \delta_{11}}{\delta_{33} - \delta_{iso}}$ is nearly zero as $\delta_{11} = \delta_{22}$ or $\delta_{22} = \delta_{33}$ (it is shown in the simulated spinning CSA sideband pattern of Figure 3a). On the contrary, asymmetry parameter is nearly 1 if the electron distribution is highly asymmetric. The value of asymmetry parameter varies as $0 \leq \eta \leq 1$.

The spin-lattice relaxation time is defined as the time taken by the spin system to evolve toward its equilibrium states by interacting with the surrounding lattice. The part of the Hamiltonian, which fluctuates with time like the dipole−dipole coupling, quadrupolar coupling, and the chemical shift anisotropy interactions, is responsible for nuclear spin relaxation. The major role in the relaxation mechanism is played

https://doi.org/10.1021/acsomega.1c03095
ACS Omega 2021, 6, 22752−22764

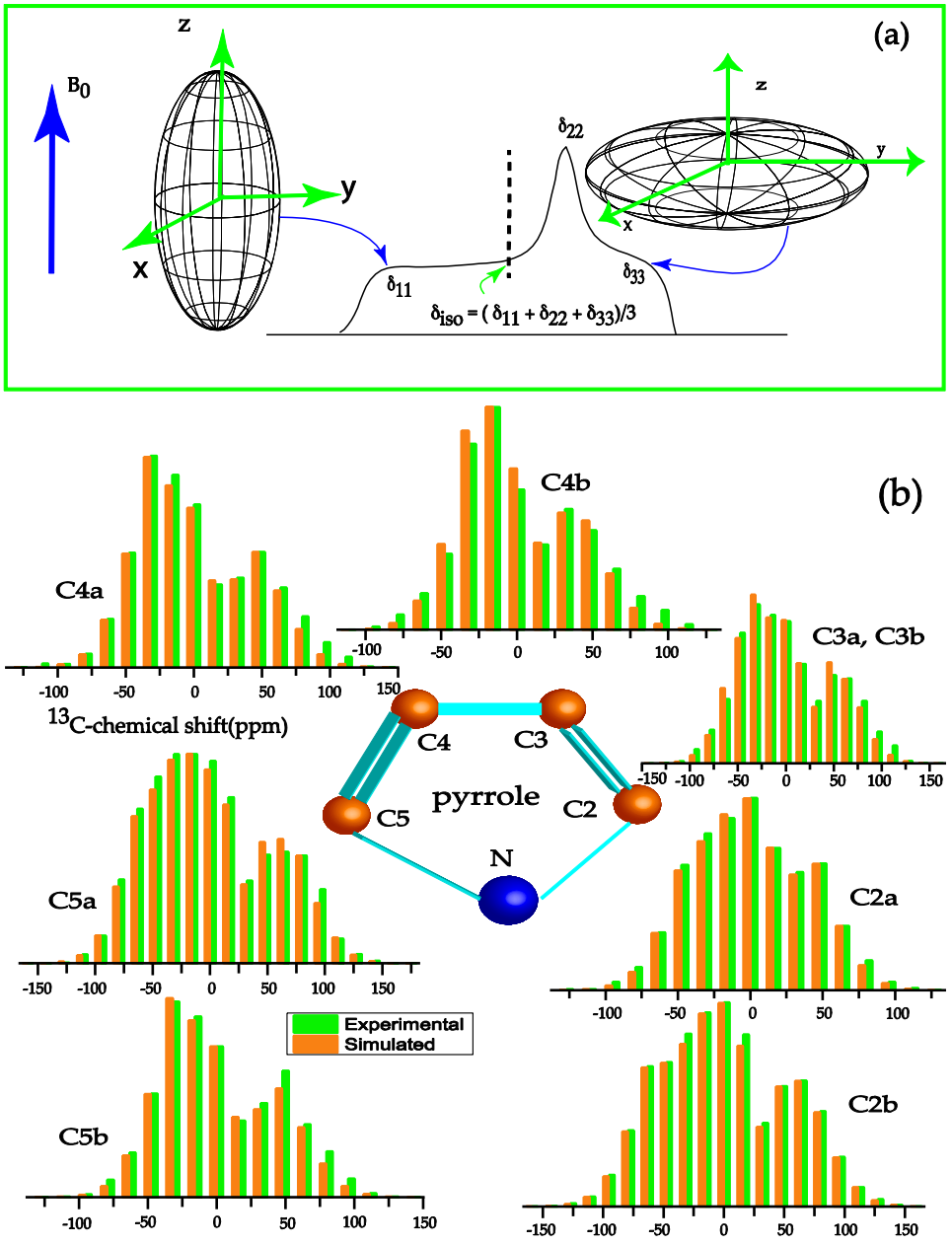

Figure 4. (a) Electron distribution around a nucleus is rarely spherically symmetric. Hence, electron density around a nucleus can be thought of as ellipsoid in shape. How much the resonance frequency of the nucleus is getting affected by the electron density depends on the orientation of this ellipsoid with respect to the external magnetic field. The chemical shift for a particular nucleus is largest when the narrowest part of the ellipsoid is orientated along the direction of the magnetic field, whereas it is smallest when the widest part of the ellipsoid is oriented along the direction of the external magnetic field. These two chemical shifts are two principal components of CSA parameters δ_{11} and δ_{33}, respectively. The third component of principal value of CSA parameter δ_{22} arises when the orientation of the ellipsoid is perpendicular to both δ_{11} and δ_{33}. (b) Spinning CSA sideband patterns at various carbon nuclei of pyrrole ring of atorvastatin calcium. At the C3 site, we can only extract the average CSA patterns of "a"- and "b"-type molecules because the isotropic chemical shift of two states coincides.

by chemical shift anisotropy and heteronuclear dipole−dipole interaction for ^{13}C carbon nuclei. It is mainly governed by the chemical shift anisotropy interaction[60−64] at the high value of the magnetic field.

The contribution of chemical shift anisotropy interaction is expressed as[60−64]

$$\frac{1}{T_1^{CSA}} = \frac{2}{15}\gamma^2 B^2 S^2 \left(\frac{\tau_2}{1+\omega^2\tau_2^2}\right) \quad (1)$$

where correlation time $\tau_c = 3\tau_2$, B is the applied magnetic field, and $S^2 = (\Delta\delta)^2\,(1 + \eta^2/3)$ and $\left[\Delta\delta = \delta_{33} - \frac{(\delta_{22}+\delta_{11})}{2}\right]$, $\left(\eta = \frac{\delta_{22}-\delta_{11}}{\delta_{33}-\delta_{iso}}\right)$.

The role of heteronuclear dipole−dipole coupling on spin-lattice relaxation mechanism is articulated as[64]

https://doi.org/10.1021/acsomega.1c03095
ACS Omega 2021, 6, 22752−22764

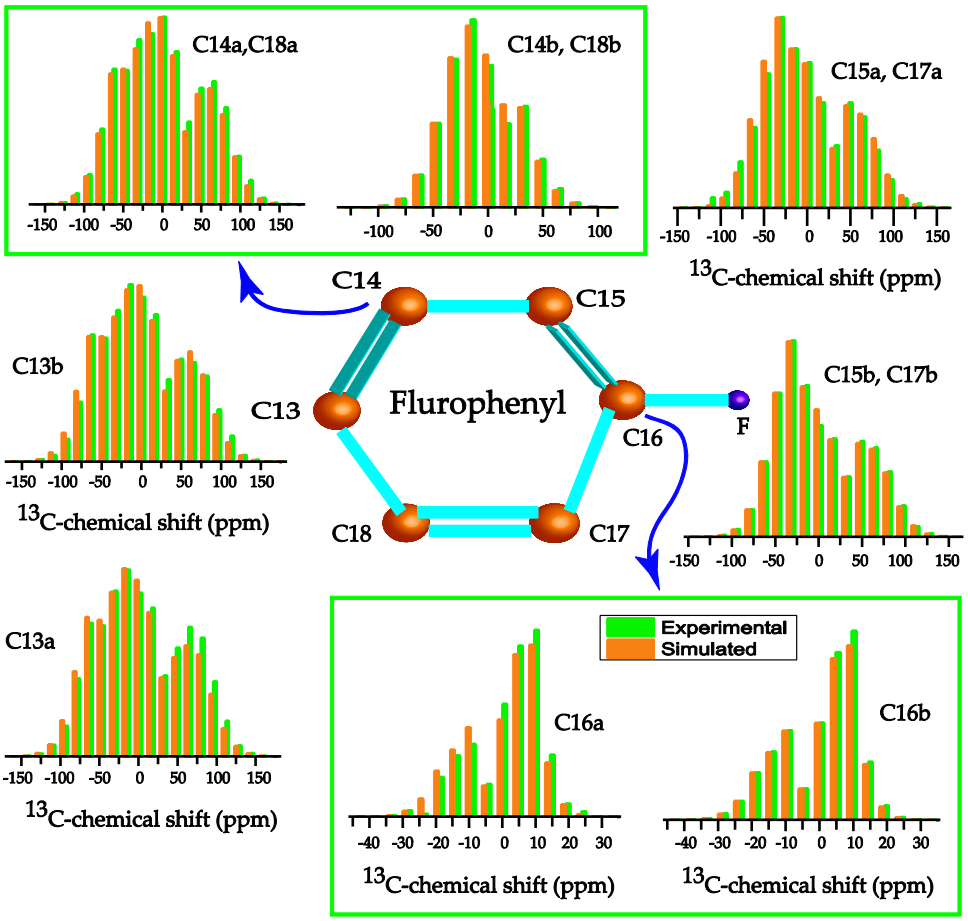

Figure 5. Spinning CSA sideband patterns of the carbon nuclei residing on the fluorophenyl ring. Generally, the values of CSA parameters are large for the carbon nuclei residing on aromatic ring due to magnetic shielding and deshielding effect, but the values of asymmetry and span are substantially lower for C16 nuclei (bonded with fluorine atom) compared to other nuclei on fluorophenyl ring. Gauche effect (hyperconjugation) is the reason behind this.[57,58] Hyperconjugation occurs due to the interaction of the electron of σ-orbital (C−H or C−C) with an adjacent antibonding σ^* orbital (C−F). Electron delocalization is associated with hyperconjugation. Remarkable variation of the spinning CSA sideband patterns is observed at C14 and C18 nuclei sites for "a"- and "b"-type molecules.

$$\frac{1}{T_1^{DD}} = \frac{1}{10}\left(\frac{\gamma_C\gamma_X\hbar}{r_{CX}^3}\right)^2 \tau_2\left[\frac{3}{1+\omega_C{}^2\tau_2^2} + \frac{1}{1+(\omega_X-\omega_C)^2\tau_2^2} + \frac{6}{1+(\omega_X+\omega_C)^2\tau_2^2}\right] \quad (2)$$

By keeping only the first term

$$\frac{1}{T_1^{DD}} = \frac{1}{10}\left(\frac{\gamma_C\gamma_X\hbar}{r_{CX}^3}\right)^2 \tau_2\left[\frac{3}{1+\omega_C{}^2\tau_2^2}\right] \quad (3)$$

where X represents any NMR-active nucleus dipolar coupled to the probe. These could be, for example, ^{1}H, ^{2}H, ^{17}O, ^{14}N, ^{15}N, etc. r_{CX} is the distance between carbon and neighboring atoms like hydrogen, oxygen, and nitrogen. This is calculated by following Ashfaq et al.[32] The contribution of heteronuclear dipole−dipole interaction on spin-lattice relaxation mechanism is inversely proportional to the sixth power of the distance between the carbon and other nuclei; therefore, only the nearest neighbor distances are taken into consideration. Larmor precession frequency $\omega = 2\pi f = 2 \times 3.14 \times 125.758$ MHz = 789.76024 MHz; $B = 11.74$ T, $\gamma_C = 10.7084$ MHz/T, $\gamma_H =$ 42.577 MHz/T, $\hbar = 1.054 \times 10^{-34}$ Js. At a high value of magnetic field, the relaxation mechanism is mainly governed by the CSA interaction. The expression of the spin-lattice relaxation rate for ^{13}C carbon is

$$\frac{1}{T_1} = \frac{1}{T_1^{CSA}} + \frac{1}{T_1^{DD}} = \frac{2}{15}\gamma^2B^2S^2\left(\frac{\tau_2}{1+\omega^2\tau_2^2}\right) + \frac{1}{10}\left(\frac{\gamma_C\gamma_X\hbar}{r_{CX}^3}\right)^2 \tau_2\left[\frac{3}{1+\omega_C{}^2\tau_2^2}\right] \quad (4)$$

2.3. Spin-Lattice Relaxation Time and Local Correlation Time at Two Independent Molecules of an Asymmetric Unit of Atorvastatin Calcium. Figure 8a,b,f shows that the longitudinal magnetization decay curves are fitted using two exponentials—one with longer relaxation time and another with shorter relaxation time for C3, C4b, C5a, C15, C19a, C21, and C32b carbon nuclei. This is the evidence of the coexistence of two different kinds of motional degrees of freedom within the molecule. The local correlation time is calculated using the expression (eq 4) for two different kinds of motional dynamics.

https://doi.org/10.1021/acsomega.1c03095
ACS Omega 2021, 6, 22752−22764

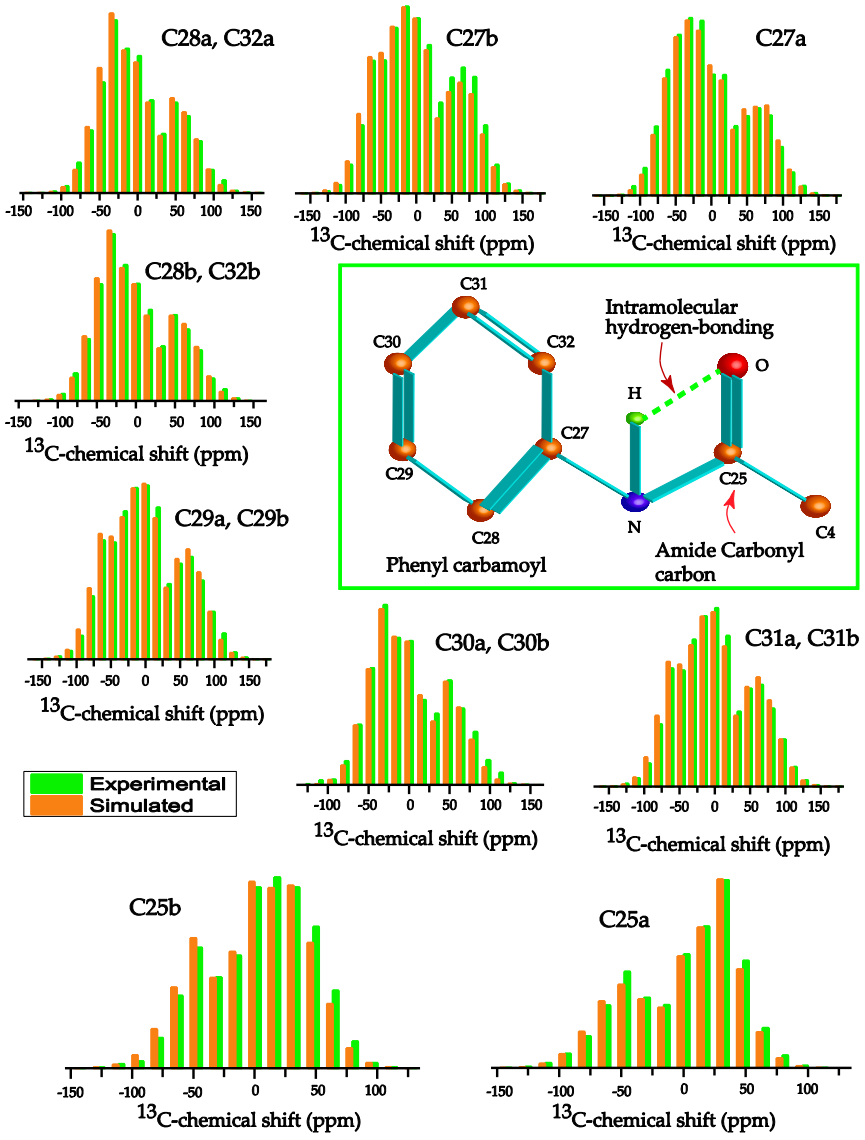

Figure 6. Spinning CSA sideband patterns of carbon nuclei residing on phenyl carbamoyl.

Table 2 and Figure 9a show that the spin-lattice relaxation time is different for "a"- and "b"-type molecules for most of the carbon nuclei like C2, C4, C5, C8, C10, and C19. The principal components of CSA parameters significantly varied for C2, C4, and C5 nuclei in two molecules of ATC-I. It is clear from Figure 10 and Table 2 that the local correlation time for those carbon nuclei sites is also varied in 1 order of magnitude. This is the first time the change in nuclear spin dynamics of two independent molecules of an asymmetric unit of ATC-I is quantified by site-specific spin-lattice relaxation measurements.

It was reported from the solid-state ^{13}C-^{1}H HETCOR experiment that the hydroxyl proton of C10 is oriented toward the carboxyl oxygen of C12, and the hydroxyl proton of C8 is oriented along the C7 for "a"-type molecule. But for "b"-type molecule, the hydroxyl protons of C8 and C10 are oriented in the same direction.[1] The orientation of the hydroxyl group of "a"-type molecule leads to a stronger hydrogen bonding compared to "b"-type molecule.[1] The CSA parameter δ_s is highly correlated with the strength of the hydrogen bonding. The decrease of the values of δ_{22} implies that the strength of the hydrogen bonding is increased.[49,54] The CSA component δ_{22} of C10 and C8 carbon nuclei is slightly lower for "a"-type molecule compared to the "b"-type molecule (as shown in Table 1, δ_{22} = 69.7 ppm for C10b, δ_{22} = 62.1 ppm for C10a; and δ_{22} = 67.9 ppm for C8b, δ_{22} = 62.8 ppm for C8a) signifies that the length of the hydrogen bond is increased in "a"-type molecule compared to "b"-type molecule. Hence, the findings of CSA measurements agree with the findings of ^{13}C-^{1}H HETCOR measurements. The CSA parameters of C11 and C12 nuclei are different, which shows that the electron distribution near the calcium ion of these two molecules is different.

The order of the local correlation time ($\tau_c = 3\tau_2$) varies significantly for the same carbon nuclei with slower spin-lattice relaxation rate and faster spin-lattice relaxation rate. Hence, each molecule of an asymmetric unit of ATC-I is associated with two different kinds of motional degrees of freedom. The coexistence of two different kinds of motional dynamics within the atorvastatin calcium molecule increases its solubility and bioavailability. Hence, the microscopic property (i.e., the existence of two different motional dynamics within the asymmetric unit) has a great influence on the macroscopic properties (like solubility and bioavailability) of the drug molecule.

https://doi.org/10.1021/acsomega.1c03095
ACS Omega 2021, 6, 22752−22764

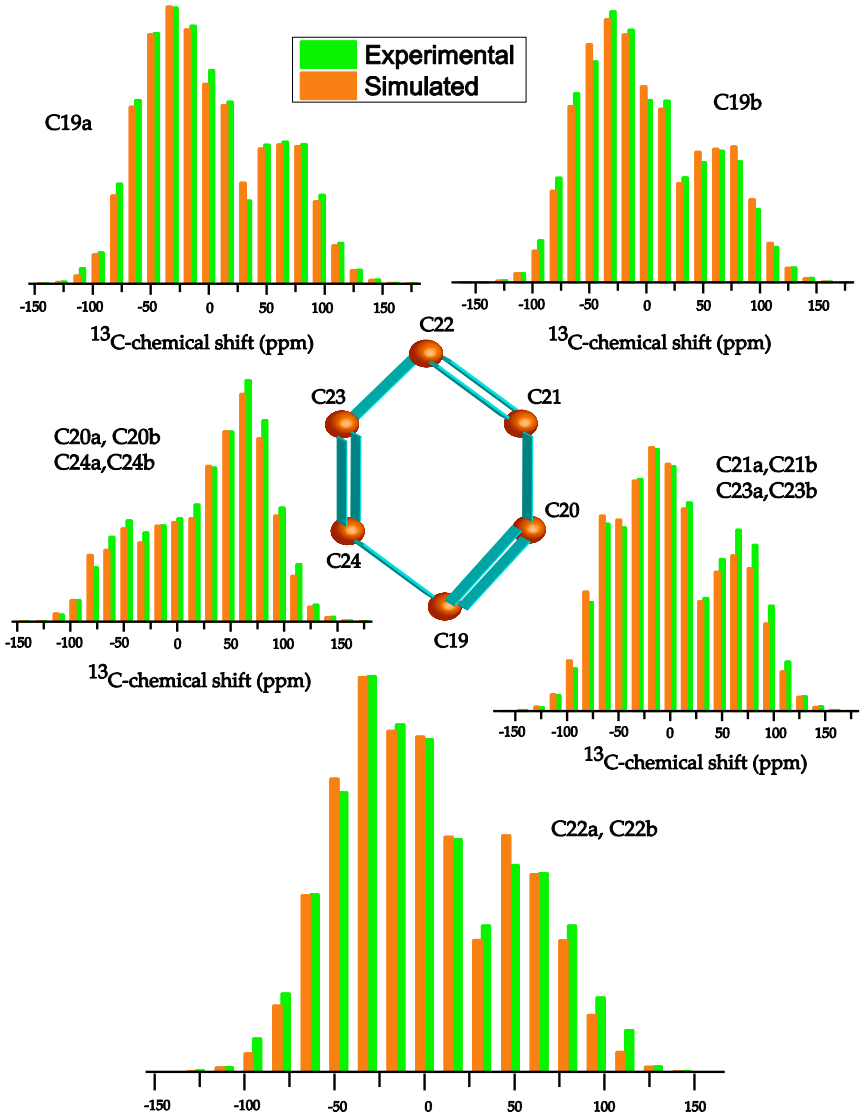

Figure 7. Spinning CSA sideband patterns of carbon nuclei residing on the phenyl ring.

Figure 10 shows that the local correlation time of "a" and "b"-type molecule varies significantly for C5, C19, C2, C4, C8, and C10 carbon nuclei sites.

3. CONCLUSIONS

A remarkable difference in the principal components of the CSA parameters and spin-lattice relaxation time is observed for "a"- and "b"-type molecules of ATC-I. This is the first time the change in the molecular dynamics of two independent molecules of an asymmetric unit of atorvastatin calcium is quantified by the Torchia CP experiment. The longitudinal magnetization decay curves are fitted using two exponentials—one with longer relaxation time and another with shorter relaxation time for C3, C4b, C5a, C15, C19a, C21, and C32b carbon nuclei. The local correlation time also varies significantly. This is the experimental evidence of the presence of two different kinds of motional degrees of freedom within the atorvastatin calcium molecule. The macroscopic properties of the drug molecule (solubility and bioavailability) are highly correlated with its microscopic property like the existence of two different kinds of molecular dynamics. The δ_{22} parameter of the carbonyl group carbon is sensitive to a change in the hydrogen bonding associated with it.[49,54] The δ_{22} values are 193.8 and 180.6 ppm for the C25 amide carbonyl group carbon of "a"- and "b"-type molecules of ATC-I, respectively, which signifies that the intramolecular hydrogen bonding (N−H·····O) associated with the "a"-type molecule is decreased compared to the "b"-type molecule. Hence, the CSA parameters of the carbonyl group carbons provide the signature of the change in hydrogen bonding of two molecules. These types of studies, in which the chemical shift anisotropy (CSA) parameters and spin-lattice relaxation time provide the information about the change in electronic distribution, density of packing, and the spin dynamics at the various crystallographic location of the drug molecule, will enrich the field NMR crystallography and provide deep insight into the dynamics of the drug molecules.

4. EXPERIMENTAL SECTION

4.1. NMR Measurements. Active pharmaceutical ingredient of atorvastatin calcium (ATC-I) was purchased from Sigma-Aldrich. ^{13}C CP-MAS SSNMR, ^{13}C Torchia CP,[17] and 2DPASS CP-MAS SSNMR[4,5] experiments were performed on a JEOL ECX 500 NMR spectrometer, associated with a 3.2 mm JEOL double-resonance MAS probe. ^{13}C CP-MAS and Torchia

https://doi.org/10.1021/acsomega.1c03095
ACS Omega 2021, 6, 22752−22764

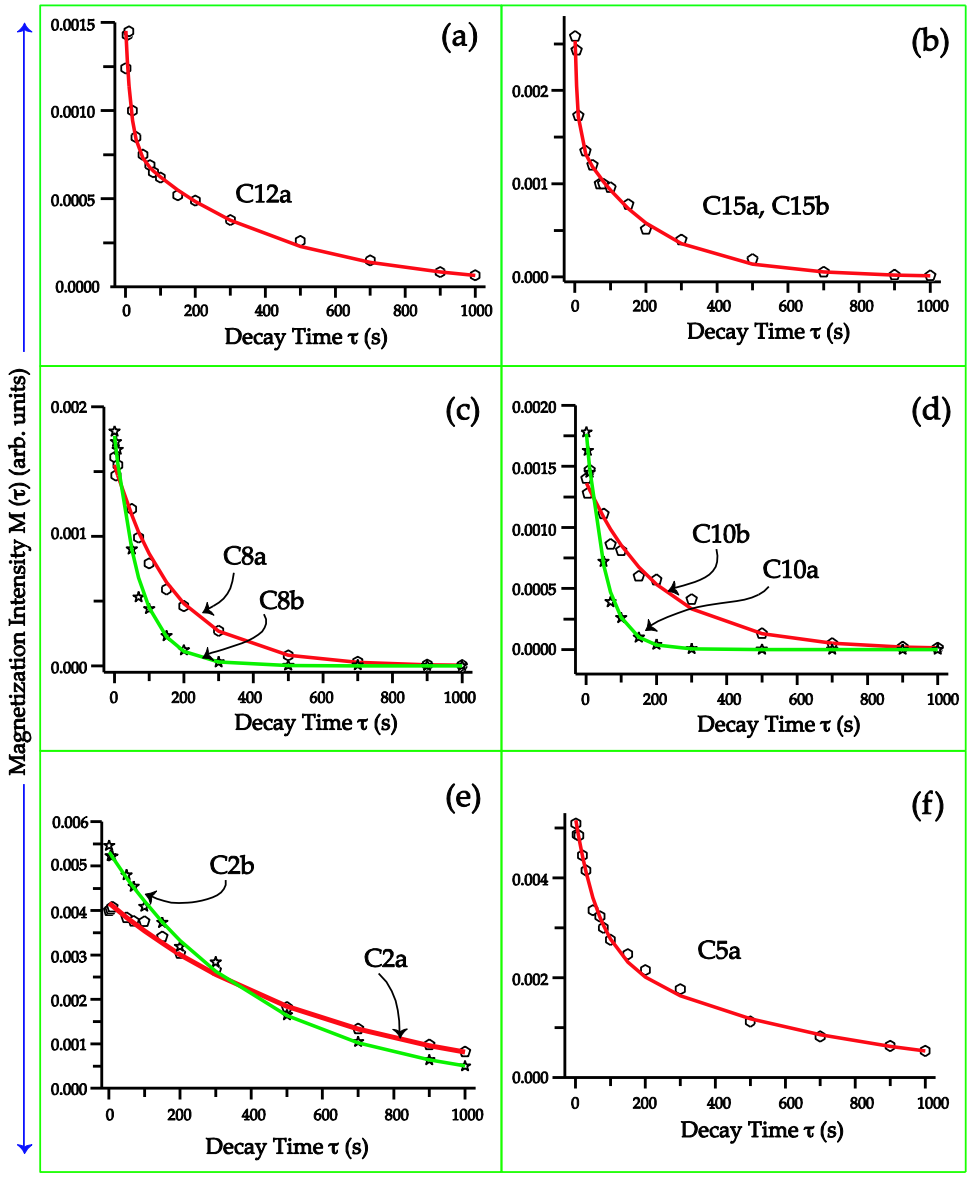

Figure 8. Longitudinal magnetization decay curves at various carbon nuclei sites of atorvastatin calcium. For (a) C12a, (b) C15a, C15b, and (f) C5a, the longitudinal magnetization curves are fitted using two exponential one with longer relaxation time and another with shorter relaxation time, which signifies that two different kinds of motional dynamics coexist within the molecule. (c–e) Spin-lattice relaxation time of two independent molecules of an asymmetric unit of atorvastatin calcium is different for certain carbon nuclei sites.

CP experiments[17] were performed at a MAS frequency of 10 kHz with SPINAL 64 ^{1}H decoupling. For the CP-MAS experiment, the contact time was 2 ms with SPINAL-64 ^{1}H decoupling. The RF magnetic field strength for ^{1}H decoupling was 100 kHz for all experiments. The number of scans for the ^{13}C CP-MAS,^{13}C 2DPASS CP-MAS, and Torchia CP experiments were 32768, 4030, and 2048 respectively. All of the experiments were performed at room temperature. The referencing for the ^{13}C spectrum is done using tetramethylsilane.

4.2. CSA Measurements. The solid-state NMR spectrum is broadened due to different types of anisotropic interactions like the chemical shift anisotropy (CSA), dipole–dipole, and quadrupolar interactions, which are averaged out in the liquid-state NMR spectrum. The data about the three-dimensional molecular structure, molecular conformation, molecular interactions, and electronic distributions are encoded in the anisotropy interaction. CSA parameters can be measured by several techniques like two-dimensional MAS/CSA NMR experiment;[18] separation of undistorted powder patterns by effortless recoupling (SUPER);[19] recoupling of chemical shift anisotropy (ROCSA);[20] γ-encoded RN_n^{ν}-symmetry-based chemical shift anisotropy (RNCSA);[21] two-dimensional magic angle flipping (2DMAF) experiment;[22−24] two-dimensional magic angle turning (2DMAT) experiment;[25] two-dimensional phase-adjusted spinning sideband cross-polarization magic angle spinning (2DPASS CP-MAS) SSNMR experiment.[4,5] The 2DPASS CP-MAS SSNMR technique is employed because this experiment is a constant-time experiment, and it can be performed in the commercially available probe, whereas for other techniques like 2DMAT, a complicated probe design is required. The evolution time is varied for the 2DMAT experiment. Hence, the data are affected by spin–spin relaxation time. The 2DPASS experiment is affected by the strong heteronuclear and homonuclear dipolar coupling effect;

https://doi.org/10.1021/acsomega.1c03095
ACS Omega 2021, 6, 22752−22764

Table 2. Spin-Lattice Relaxation Time and Local Correlation Time of Two Independent Molecules of an Asymmetric Unit of Atorvastatin Calcium (Referred as Molecules "a" and "b" by Following Wang et al.[1]) at Crystallographically Different Carbon Sites

a-type molecule			b-type molecule		
carbon nuclei	spin-lattice relaxation time (s)	local correlation time (s)	carbon nuclei	spin-lattice relaxation time (s)	local correlation time (s)
C12a	325 ± 20	$3.1 \times 10^{-4} \pm 6.3 \times 10^{-7}$	C12b	400 ± 25	$4.5 \times 10^{-4} \pm 9.5 \times 10^{-7}$
				15 ± 2	$1.7 \times 10^{-5} \pm 7.6 \times 10^{-8}$
C25a	342 ± 20	$5.5 \times 10^{-4} \pm 1.0 \times 10^{-7}$	C25b	342 ± 20	$5.3 \times 10^{-4} \pm 1.7 \times 10^{-7}$
C5a	630 ± 50	$1.4 \times 10^{-3} \pm 2.3 \times 10^{-7}$	C5b	470 ± 50	$6.6 \times 10^{-4} \pm 2.3 \times 10^{-7}$
	65 ± 5	$2.6 \times 10^{-7} \pm 2.6 \times 10^{-9}$			
C19a	755 ± 50	$1.8 \times 10^{-3} \pm 1.7 \times 10^{-7}$	C19b	422 ± 20	$1 \times 10^{-3} \pm 1.4 \times 10^{-7}$
	95 ± 5	$2.3 \times 10^{-4} \pm 1.2 \times 10^{-7}$			
C20a	515 ± 50	$2.8 \times 10^{-3} \pm 1.7 \times 10^{-7}$	C20b	595 ± 50	$3.1 \times 10^{-3} \pm 5.3 \times 10^{-7}$
				34 ± 5	$8.8 \times 10^{-5} \pm 1.6 \times 10^{-8}$
C21a	650 ± 50	$1.5 \times 10^{-3} \pm 3.3 \times 10^{-7}$	C21b	650 ± 50	$1.5 \times 10^{-3} \pm 2.7 \times 10^{-7}$
	40 ± 5	$9.4 \times 10^{-5} \pm 2.7 \times 10^{-8}$		40 ± 5	$9.4 \times 10^{-5} \pm 2.1 \times 10^{-8}$
C2a	614 ± 50	$6.7 \times 10^{-4} \pm 1.8 \times 10^{-7}$	C2b	424 ± 50	$8.6 \times 10^{-4} \pm 1.2 \times 10^{-7}$
C3a	460 ± 20	$8.3 \times 10^{-4} \pm 4.3 \times 10^{-7}$	C3b	460 ± 20	$8.3 \times 10^{-4} \pm 5.3 \times 10^{-7}$
	15 ± 5	$2.7 \times 10^{-5} \pm 1.6 \times 10^{-8}$		15 ± 5	$2.7 \times 10^{-5} \pm 3.6 \times 10^{-8}$
C4a	560 ± 50	$8.1 \times 10^{-4} \pm 3.6 \times 10^{-7}$	C4b	430 ± 20	$2.9 \times 10^{-4} \pm 1.2 \times 10^{-7}$
				23 ± 5	$2.6 \times 10^{-5} \pm 4.3 \times 10^{-8}$
C32a	390 ± 20	$7.4 \times 10^{-4} \pm 2.9 \times 10^{-7}$	C32b	350 ± 20	$6.8 \times 10^{-4} \pm 4.3 \times 10^{-7}$
	20 ± 5	$3.8 \times 10^{-5} \pm 1.7 \times 10^{-8}$			
C15a	210 ± 10	$4.2 \times 10^{-4} \pm 1.9 \times 10^{-7}$	C15b	210 ± 10	$4.2 \times 10^{-4} \pm 2.4 \times 10^{-7}$
	7 ± 1	$1.4 \times 10^{-5} \pm 3.2 \times 10^{-8}$		7 ± 1	$1.4 \times 10^{-5} \pm 2.3 \times 10^{-8}$
C10a	52 ± 5	$9.1 \times 10^{-6} \pm 1.9 \times 10^{-9}$	C10b	212 ± 10	$3.5 \times 10^{-5} \pm 3.9 \times 10^{-8}$
C8a	170 ± 10	$3.8 \times 10^{-5} \pm 1.5 \times 10^{-8}$	C8b	72 ± 5	$1.4 \times 10^{-5} \pm 1.2 \times 10^{-8}$

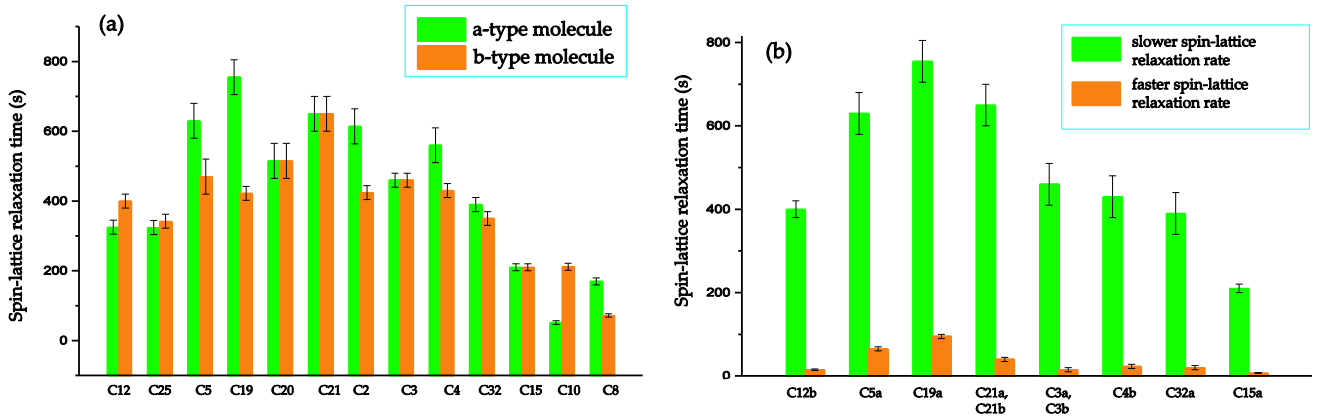

Figure 9. Bar diagram of (a) the spin-lattice relaxation time at various carbon nuclei sites of "a"- and "b"-type molecules. A significant difference in spin-lattice relaxation time is observed at C12, C5, C19, C2, C4, C32, C8, and C10. (b) Longitudinal magnetization decay is fitted using two exponential—one with longer relaxation time and another with shorter relaxation time for C12b, C5a, C19a, C21, C3, C4b, C32a, and C15a. This is the experimental evidence of the presence of two different kinds of motional dynamics within ATC-I.

however, in this case, the heteronuclear and homonuclear dipolar couplings are the negligible factors due to the low natural abundance (~1.1%) of ^{13}C nucleus.

The broadening due to chemical shift anisotropy interaction is nullified by spinning the rotor at the magic angle spinning (MAS) frequency greater than the span of the chemical shift anisotropy at the cost of losing the information about the three-dimensional molecular conformation, molecular dynamics, and electron distribution surrounding the nucleus. One of the ways to retrieve the principal components of the CSA parameters is to reduce the MAS frequency less than the span of the chemical shift anisotropy. Under this condition, the solid-state NMR spectrum is flanked on both sides of the isotropic chemical shift by sidebands equally spaced at the MAS frequency. The 2DPASS CP-MAS SSNMR experiment is a useful technique to simplify the solid-state MAS NMR spectrum containing complicated spinning sideband manifolds. Herzfeld and Berger had derived graphical and numerical methods for evaluating the principal components of the CSA tensor from the intensities of the sidebands.[26] The pulse sequence of the 2DPASS SSNMR experiment consists of five π-pulses. The total duration of five π-pulses remains unchanged throughout the experiment. The time intervals among five π-pulses are followed by the PASS equation as reported by Antzutkin et al.[4] This experiment correlates the isotropic dimension with the anisotropic dimension.

The direct dimension of the 2D spectrum yields an infinite spinning speed spectrum with no sideband. The 2DPASS CP-MAS SSNMR experiments were performed at MAS frequencies

https://doi.org/10.1021/acsomega.1c03095
ACS Omega 2021, 6, 22752−22764

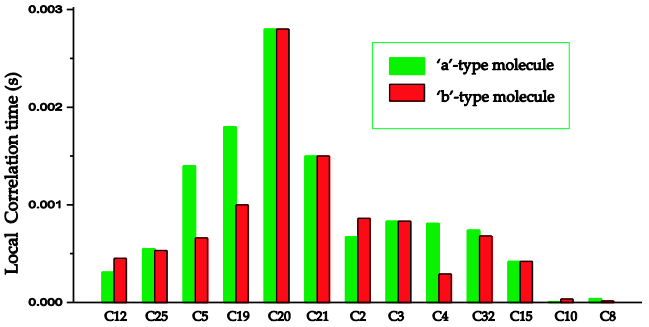

Figure 10. Bar diagram of the local correlation time at various carbon nuclei sites in two independent molecules of an asymmetric unit of ATC-I. A significant difference in local correlation time is observed at C12, C5, C19, C2, C4, C32, C8, and C10.

of 600 Hz and 2 kHz. The pulse length of the ^{13}C nucleus at 90° was 3.3 us. The relaxation delay was 15 s. A 13-step cogwheel phase cycling COG13(0, 1, 0, 1, 0, 1; 0, 6) was used.[27,28] The number of scans for the 2DPASS CP-MAS SSNMR experiments was 4030 (integral multiple of 13). The coherence transfer pathway for the 2DPASS NMR experiment was reported by Ghosh et al.[7] A total of 16 data points were acquired in the indirect dimension as the numbers of sidebands were less than 16. The anisotropic part of the chemical shift interaction in natural abundance ^{13}C spin-1/2 nuclei (for those nuclei where the homonuclear dipole−dipole coupling is much less than the rotor frequency) evolves during the PASS sequence under the rotor pitch evolution in the t1 dimension.

■ ASSOCIATED CONTENT

Supporting Information

The Supporting Information is available free of charge at https://pubs.acs.org/doi/10.1021/acsomega.1c03095.

^{13}C Frequency (ppm) (Figure S1) (PDF)
Isotropic chemical shift (ppm) (Figure S2) (PDF)
Simulated spinning CSA sideband pattern (Figure S3) (PDF)
Experimental simulated (Figure S4) (PDF)
Fluorophenyl ring (Figure S5) (PDF)
Intramolecular hydrogen bonding (Figure S6) (PDF)
Frequency ppm (Figure S7) (PDF)
Magnetization intensityFigure S8 (PDF)
Spin-lattice relaxation time (s) (Figure S9) (PDF)
Local correlation time (Figure S10) (PDF)

■ AUTHOR INFORMATION

Corresponding Author

Manasi Ghosh − *Physics Section, Mahila Maha Vidyalaya, Banaras Hindu University, Varanasi 221005 Uttar Pradesh, India;* orcid.org/0000-0002-8472-0288; Email: manasi.ghosh@bhu.ac.in

Authors

Krishna Kishor Dey − *Department of Physics, Dr. Harisingh Gour Central University, Sagar 470003 Madhya Pradesh, India*

Lekhan Lodhi − *Department of Zoology, Dr. Harisingh Gour Central University, Sagar 470003 Madhya Pradesh, India*

Complete contact information is available at: https://pubs.acs.org/10.1021/acsomega.1c03095

Notes

The authors declare no competing financial interest.

■ ACKNOWLEDGMENTS

Manasi Ghosh is grateful to Science and Engineering Research Board (SERB), Department of Science and Technology (DST), Government of India (file no. EMR/2016/000249), and SERB-POWER Grant (file no. SPG/2021/000303) for financial support. The authors are thankful to the Sophisticated Instrumentation Centre (SIC) of Dr. Harisingh Gour Central University for providing solid-state NMR facility.

■ REFERENCES

(1) Wang, W. D.; Gao, X.; Strohmeier, M.; Wang, W.; Bai, S.; Dybowski, C. Solid-State NMR Studies of Form I of Atorvastatin Calcium. *J. Phys. Chem. B* **2012**, *116*, 3641−3649.
(2) Holmes, S. T.; Wang, W. D.; Hou, G.; Dybowski, C.; Wang, W.; Bai, S. A New NMR Crystallographic Approach to Reveal the Calcium Local Structure of Atorvastatin Calcium. *Phys. Chem. Chem. Phys.* **2019**, *21*, 6319−6326.
(3) Bai, S.; Quinn, C. M.; Holmes, S. T.; Dybowski, C. High-resolution 13C and 43Ca solid-state NMR and computational studies of the ethylene glycol solvate of atorvastatin calcium. *Magn. Reson. Chem.* **2020**, *58*, 1010−1017.
(4) Antzutkin, O. N.; Shekar, S. C.; Levitt, M. H. Two-dimensional sideband separation in magic angle spinning NMR. *J. Magn. Reson., Ser. A* **1995**, *115*, 7−19.
(5) Dixon, W. T. Spinning-sideband-free and spinning-sideband-only NMR spectra in spinning samples. *J. Chem. Phys.* **1982**, *77*, 1800−1809.
(6) Bhowal, R.; Balaraman, A. A.; Ghosh, M.; Dutta, S.; Dey, K. K.; Chopra, D. Probing atomistic behaviour to unravel dielectric phenomena in charge transfer cocrystal. *J. Am. Chem. Soc.* **2021**, *143*, 1024−1037.
(7) Ghosh, M.; Sadhukhan, S.; Dey, K. K. Elucidating the internal structure and dynamics of α-chitin by 2DPASS-MAS-NMR and spin-lattice relaxation measurements. *Solid State Nucl. Magn. Reson.* **2019**, *97*, 7−16.
(8) Ghosh, M.; Prajapati, B. P.; Kango, N.; Dey, K. K. A comprehensive and comparative study of the internal structure and dynamics of natural β-keratin and regenerated β-keratin by solid state NMR spectroscopy. *Solid State Nucl. Magn. Reson.* **2019**, *101*, 1−11.
(9) Ghosh, M.; Kango, N.; Dey, K. K. Investigation of the internal structure and dynamics of cellulose by ^{13}C-NMR relaxometry and 2DPASS-MAS-NMR measurements. *J. Biomol. NMR* **2019**, *73*, 601−616.
(10) Dey, K. K.; Ghosh, M. Understanding the effect of deacetylation on chitin by measuring chemical shift anisotropy tensor and spin lattice relaxation time. *Chem. Phys. Lett.* **2020**, *738*, No. 136782.
(11) Dey, K. K.; Gayen, S.; Ghosh, M. Investigation of the detailed internal structure and dynamics of itraconazole by solid-state NMR measurements. *ACS Omega* **2019**, *4*, 21627−21635.
(12) Dey, K. K.; Gayen, S.; Ghosh, M. Understanding the correlation between structure and dynamics of clocortolonepivalate by solid state NMR measurement. *RSC Adv.* **2020**, *10*, 4310−4321.
(13) Ghosh, M.; Gayen, S.; Dey, K. K. An atomic resolution description of folic acid by solid state NMR measurements. *RSC Adv.* **2020**, *10*, 24973−24984.
(14) Dey, K. K.; Ghosh, M. Determination of the Correlation between the Structure and Dynamics of Deflazacort by solid state NMR measurements. *New J. Chem.* **2020**, *44*, 18419−18430.
(15) Dey, K. K.; Ghosh, M. Determination of Chemical Shift Anisotropy Tensor and Molecular Correlation Time of Proton Pump Inhibitor Omeprazole by Solid State NMR Measurements. *New J. Chem.* **2020**, *44*, 19393−19403.
(16) Dey, K. K.; Ghosh, M. Investigation of the Structure and Dynamics of Antiviral Drug Adefovir Dipivoxil by Site-Specific Spin−Lattice Relaxation Time Measurements and Chemical Shift Anisotropy Tensor Measurements. *ACS Omega* **2020**, *5*, 29373.

(17) Torchia, D. A. The measurement of proton-enhanced carbon-13 T1 values by method which suppresses artifacts. *J. Magn. Reson.* **1978**, *30*, 613−616.
(18) Tycko, R.; Dabbagh, G.; Mirau, P. A. Determination of chemical shift anisotropy lineshapes in a two-dimensional magic angle spinning NMR experiment. *J. Magn. Reson. (1969)* **1989**, *85*, 265−274.
(19) Liu, S. F.; Mao, J. D.; Schmidt-Rohr, K. A robust technique for two-dimensional separation of undistorted chemical shift anisotropy powder patterns in magic angle spinning NMR. *J. Magn. Reson.* **2002**, *155*, 15−28.
(20) Chan, J. C. C.; Tycko, R. Recoupling of chemical shift anisotropies in solid state NMR under high speed magic angle spinning and in uniformly ^{13}C labelled systems. *J. Chem. Phys.* **2003**, *118*, 8378−8389.
(21) Hou, G.; Byeon, In-Ja L.; Ahn, J.; Gronenborn, A. M.; Polenova, T. Recoupling of chemical shift anisotropy by R-symmetry sequences in magic angle spinning NMR spectroscopy. *J. Chem. Phys.* **2012**, *137*, 134201−134210.
(22) Bax, A. D.; Szeverenyi, N. M.; Maciel, G. E. Chemical shift anisotropy in powdered solids studied by 2D FT NMR with flipping of the spinning axis. *J. Magn. Reson. (1969)* **1983**, *55*, 494−497.
(23) Bax, A. D.; Szeverenyi, N. M.; Maciel, G. E. Correlation of isotropic shifts and chemical shift anisotropies by two-dimensional Fourier-transform magic angle hopping NMR spectroscopy. *J. Magn. Reson. (1969)* **1983**, *52*, 147−152.
(24) Bax, A. D.; Szeverenyi, N. M.; Maciel, G. E. Chemical shift anisotropy in powdered solids studied by 2D FT CP/MAS NMR. *J. Magn. Reson. (1969)* **1983**, *51*, 400−408.
(25) Gan, Z. High-resolution chemical shift and chemical shift anisotropy correlation in solids using slow magic angle spinning. *J. Am. Chem. Soc.* **1992**, *114*, 8307−8309.
(26) Herzfeld, J.; Berger, A. E. Sideband intensities in NMR spectra of samples spinning at the magic angle. *J. Chem. Phys.* **1980**, *73*, 6021−6030.
(27) Ivchenko, N.; Hughes, C. E.; Levitt, M. H. Application of cogwheel phase cycling to sideband manipulation experiments in solid-state NMR. *J. Magn. Reson.* **2003**, *164*, 286−293.
(28) Levitt, M. H.; Madhu, P. K.; Hughes, C. E. Cogwheel Phase Cycling. *J. Magn. Reson.* **2002**, *155*, 300−306.
(29) Sonje, V. M.; Kumar, L.; Meena, C. L.; Kohli, G.; Puri, V.; Jain, R.; Bansal, A. K.; Brittain, H. G. Chapter-1 Atorvastatin calcium. *Profiles Drug Subst., Excipients, Relat. Methodol.* **2010**, *35*, 1−70.
(30) Skorda, D.; Kontoyannis, C. G. Identification and quantitative determination of Atorvastatin calcium polymorph in tablets using FT-Raman spectroscopy. *Talanta* **2008**, *74*, 1066−1070.
(31) Shete, G.; Puri, V.; Kumar, L.; Bansal, A. K. Solid State Characterization of Commercial Crystalline and Amorphous Atorvastatin Calcium Samples. *AAPS PharmSciTech* **2010**, *11*, 598−609.
(32) Ashfaq, M.; Tahir, M. N.; Khan, I. U.; Iqbal, M. S.; Arshad, M. N. Degradation of atorvastatin: (1R,2S,4S,5S)-4-(4-fluorophenyl)-2-hydroperoxy-4-hydroxy-2-isopropyl-N,5- diphenyl-3,6-dioxabicyclo[3.1.0]hexane1-carboxamide. *Acta Crystallogr., Sect. E: Struct. Rep. Online* **2008**, *64*, o1548.
(33) Ramsey, N. F. Magnetic Shielding of Nuclei in Molecules. *Phys. Rev.* **1950**, *78*, 699−703.
(34) Ramsey, N. F. Chemical effects in nuclear magnetic resonance and in diamagnetic susceptibility. *Phys. Rev.* **1952**, *86*, 243−246.
(35) Haeberlen, U. *High Resolution NMR in Solids: Selective Averaging*; Academic Press: New York, 1976.
(36) Wylie, B. J.; Rienstra, C. M. Multidimensional solid state NMR of anisotropic interactions in peptides and proteins. *J. Chem. Phys.* **2008**, *128*, No. 052207.
(37) Shoji, A.; Ando, S.; Kuroki, S.; Ando, I.; G A Webb, G. A. *Annu. Rep. NMR Spectrosc.* **1993**, *26*, 55−98.
(38) Veeman, W. S. Carbon-13 Chemical Shift Anisotropy. *Prog. Nucl. Magn. Reson. Spectrosc.* **1984**, *16*, 193−235.
(39) Shao, L.; Titman, J. J. Chemical Shift Anisotropy Amplification. *Prog. Nucl. Magn. Reson. Spectrosc.* **2007**, *51*, 103−137.
(40) Wu, G. Solid-state 17O NMR studies of organic and biological molecules. *Prog. Nucl. Magn. Reson. Spectrosc.* **2008**, *52*, 118−169.
(41) *Solid State NMR of Polymers*; Ando, I.; Asakura, T., Eds.; Elsevier Science: Amsterdam, 1998.
(42) *Solid-State NMR Spectroscopy: Principles and Applications*; Antzutkin, O. N.; Duer, M. J., Eds.; Blackwell Sciences: Oxford, 2002; p 280.
(43) *NMR Spectroscopy of Biological Solids*; Ramamoorthy, A., Ed.; CRC Press: Cleveland, 2005.
(44) Gerstein, B. C.; Dybowski, C. R. *Transient Techniques in NMR of Solids, An Introduction to Theory and Practice*; Academic Press: Orlando, 1985.
(45) Antzutkin, O. N. Sideband manipulation in magic-angle-spinning nuclear magnetic resonance. *Prog. Nucl. Magn. Reson. Spectrosc.* **1999**, *35*, 203−266.
(46) Duncan, T. M. *A Compilation of Chemical Shift Anisotropics*; The Farragut Press: Chicago, 1990.
(47) de Dios, A. C. Ab initio calculations of the NMR chemical shift. *Prog. Nucl. Magn. Reson. Spectrosc.* **1996**, *29*, 229−278.
(48) Sen, S. Dynamics in Inorganic Glass-forming Liquids by NMR Spectroscopy. *Prog. Nucl. Magn. Reson. Spectrosc.* **2020**, *116*, 155−176.
(49) Saitô, H.; Ando, I.; Ramamoorthy, A. Chemical shift tensor-the heart of NMR: Insight into biological aspects of proteins. *Prog. Nucl. Magn. Reson. Spectrosc.* **2010**, *57*, 181−228.
(50) Laws, D. D.; Bitter, H. M. L.; Jerschow, A. Solid-State NMR Spectroscopic Methods in Chemistry. *Angew. Chem., Int. Ed.* **2002**, *41*, 3096−3129.
(51) Duer, M. J. *Solid State NMR Spectroscopy Principles and Applications*; Blackwell science, 2007.
(52) McConnell, H. M. Theory of Nuclear Magnetic Shielding in Molecules: Long-Range Dipolar Shielding of protons. *J. Chem. Phys.* **1957**, *27*, No. 226.
(53) Abraham, R. J.; Mobli, M.; Smith, R. J. 1H chemical shifts in NMR: Carbonyl anisotropies and steric effect in aromatic aldehydes and ketones. *Magn. Reson. Chem.* **2003**, *41*, 26−36.
(54) Asakawa, N.; Kameda, T.; Kuroki, S.; Kurosu, H.; Ando, S.; Ando, I.; Shoji, A. Structural Studies of Hydrogen-bonded Peptides and Polypeptides by Solid-state NMR. *Annu. Rep. NMR Spectrosc.* **1998**, *35*, 55−137.
(55) O'Hagan, D. Understanding organofluorine chemistry. An introduction to the C−F bond. *Chem. Soc. Rev.* **2008**, *37*, 308−319.
(56) Goodman, L.; Gu, H.; Pophristic, V. Gauche effect in 1,2-Difluoroethane. hyperconjugation, bent bonds, steric repulsion. *J. Phys. Chem. A* **2005**, *109*, 1223−1229.
(57) Weinhold, F. *The Encyclopedia of Computational Chemistry*; Schleyer, P. V. R.; Allinger, N. L.; Clark, T.; Gasteiger, J.; Kollman, P. A.; Schaefer, H. F., III; Schreiner, P. R., Eds.; John Wiley & Sons: Chichester, U.K., 1998; pp 1792−1811.
(58) Wiberg, K. B.; Murcko, M. A.; K E Laidig, K. E.; MacDougall, P. J. Origin of the "Gauche Effect" in substituted ethanes and ethenes. *J. Phys. Chem. A.* **1990**, *94*, 6956−6959.
(59) Wiberg, K. B. Bent bonds in organic compounds. *Acc. Chem. Res.* **1996**, *29*, 229−234.
(60) Nicholas, M. P.; Eryilmaz, E.; Ferrage, F.; Cowburn, D.; Ghose, R. Nuclear spin relaxation in isotropic and anisotropic media. *Prog. Nucl. Magn. Reson. Spectrosc.* **2010**, *57*, 111−158.
(61) Orendt, A. M.; Facelli, J. C. Solid state effects on NMR chemical shifts. *Annu. Rep. NMR Spectrosc.* **2007**, *62*, 115−178.
(62) Tjandra, N.; Szabo, A.; Bax, Ad. Protein backbone dynamics and 15B chemical shift anisotropy from quantitative measurement of relaxation interference effects. *J. Am. Chem. Soc.* **1996**, *118*, 6986−6991.
(63) Dais, P.; Spyros, A. ^{13}C nuclear magnetic relaxation and local dynamics of synthetic polymers in dilute solution and in the bulk state. *Prog. Nucl. Magn. Reson. Spectrosc.* **1995**, *27*, 555−633.
(64) Anet, F. A. L.; O'Leary, D. J. The shielding tensor Part II: Understanding its strange effect on relaxation. *Concepts Magn. Reson.* **1992**, *4*, 35−52.

https://doi.org/10.1021/acsomega.1c03095
ACS Omega 2021, 6, 22752−22764